Laminar Flow at the Trailing Edge of a Flat Plate

H. C. Chen* and V. C. Patel†
University of Iowa, Iowa City, Iowa

Numerical solutions of the Navier-Stokes equations for laminar flow around and beyond the trailing edge of a flat plate at a Reynolds number of 10^5 are presented. The size of the computational domain has been varied over a wide range to show that previous calculations of this type have employed domains which were too small to obtain a domain-independent solution. The present large-domain solutions are compared with those obtained with the triple-deck and interactive boundary-layer theories. Satisfactory agreement is found in regions of validity of these theories. However, the present results are more complete insofar as they extend well into the asymptotic wake.

I. Introduction

THE classical problem of incompressible laminar flow over a flat plate aligned with a uniform stream has been the subject of numerous investigations. When the Reynolds number, $R = UL/\nu$, where U is the freestream velocity, L is the plate length, and ν is the kinematic viscosity of the fluid, is large, the boundary layer on the plate is described by the Blasius solution. However, it is well known that this solution is not valid in the neighborhood of the leading and trailing edges due to the breakdown of the approximations made in boundary-layer theory.

The flow over the trailing edge and in the near wake has attracted much attention particularly since the formulation of the triple-deck theory by Stewartson[1] and Messiter[2] for the limiting case of $R \to \infty$. According to this theory, there are three layers (decks) near the trailing edge, in each of which the Navier-Stokes equations can be approximated in different ways. For the case of a flat plate, numerical solutions of the triple-deck equations have been presented by Jobe and Burggraf,[3] Melnik and Chow[4] and Veldman and van de Vooren,[5] and since then, the triple-deck formulation has been extended to asymmetric trailing edges, the flow in the neighborhood of separation, shock boundary-layer interaction, and even to turbulent flows.

Two other approaches have also been used in the treatment of trailing-edge and near-wake flows. The first is the classical approach of viscous-inviscid interactions, in which the boundary-layer and wake solutions are matched with the external inviscid flow by interactive means. This has gained considerable popularity in recent years. McDonald and Briley[6] have presented a review of this approach with particular emphasis on the so-called inverse boundary-layer calculation methods. The physical assumption underlying these methods is that the boundary-layer equations are valid over the trailing edge (and even in regions of "small" separation). The singularity of these equations in the direct mode (at the trailing edge and at separation) is avoided by the interaction with the external flow provided appropriate solution algorithms are used. The second approach seeks numerical solutions of either the complete Navier-Stokes equations or the less general partially-parabolic (or "parabolized" or "semi-elliptic" Navier-Stokes) equations.

This paper is concerned with the solution of the Navier-Stokes equations using an extension of a numerical method which has been developed for the solution of the partially parabolic equations for application to laminar and turbulent flows around complex three-dimensional bodies. Although the extended method can be used also for such flows, the application to the simple case of two-dimensional laminar flow at the trailing edge of a flat plate is motivated by the need to establish the method's capabilities and limitations by comparison with solutions obtained by other means. A systematic study of the influence of the boundary conditions and the size of the numerical-solution domain is made to explore the extent of the viscous-inviscid interaction at the trailing edge at a Reynolds number of 10^5. Comparisons with other solutions at this Reynolds number show that solution domains employed in previous numerical studies may have been too small to capture the entire viscous-inviscid interaction. Some defects of the commonly accepted triple-deck solutions are also identified.

II. Outline of the Solution Procedures

A detailed description of the general numerical approach employed here is given in Chen and Patel.[7] For general applications, the method uses numerically generated coordinates, solves the partially parabolic transport equations for the velocity components and turbulence parameters by the finite-analytic scheme of Chen and Chen,[8,9] and uses a two-step global algorithm to obtain the pressure by satisfying the continuity equation. It is a multi-sweep, time-marching scheme which can be used for steady as well as unsteady flows, and can be readily extended to fully elliptic equations. For the problem considered here, the turbulence model is suppressed but the method has beem extended to the full Navier-Stokes equations. However, the structure of the basic method is retained intact. Thus, the computational grid is generated numerically although it is recognized that much simpler alternatives are available for the case of a flat plate. In a similar vein, the original formulation in primitive variables is retained while recognizing that suitable transformations for this simple problem can be devised to ensure better accuracy and numerical efficiency. In the following, we shall briefly describe the equations and solution procedures as they apply to the flat plate.

A. Equations

In Cartesian (x,y) coordinates with the origin at the leading edge, x along the plate, and y normal to it, the Navier-Stokes equations are:

$$\frac{\partial u}{\partial t} + u\frac{\partial u}{\partial x} + v\frac{\partial u}{\partial y} = -\frac{\partial p}{\partial x} + \frac{1}{R}\left(\frac{\partial^2 u}{\partial x^2} + \frac{\partial^2 u}{\partial y^2}\right) \quad (1)$$

Received Jan. 22, 1986; revision received Nov. 19, 1986.

*Assistant Research Scientist, Iowa Institute of Hydraulic Research. Member AIAA.
†Professor of Mechanical Engineering. Member AIAA.

$$\frac{\partial v}{\partial t}+u\frac{\partial v}{\partial x}+v\frac{\partial v}{\partial y}=-\frac{\partial p}{\partial y}+\frac{1}{R}\left(\frac{\partial^2 v}{\partial x^2}+\frac{\partial^2 v}{\partial y^2}\right) \quad (2)$$

$$\frac{\partial u}{\partial x}+\frac{\partial v}{\partial y}=0 \quad (3)$$

where the velocity components (u,v), pressure p, time t, and coordinates (x,y) are nondimensionalized in the usual way by the freestream velocity U, the plate length L, and fluid density ρ, $R=UL/\nu$ is the Reynolds number and ν is the kinematic viscosity.

B. Numerical Grid

The foregoing equations are solved in transformed coordinates (ξ,η) which are defined by the Poisson equations:

$$\frac{\partial^2 \xi}{\partial x^2}+\frac{\partial^2 \xi}{\partial y^2}=f^1(\xi,\eta) \quad (4)$$

$$\frac{\partial^2 \eta}{\partial x^2}+\frac{\partial^2 \eta}{\partial y^2}=f^2(\xi,\eta) \quad (5)$$

where f^1 and f^2 are the grid-control functions which are chosen a priori to obtain the desired distribution of points in the physical (x,y) space. The grid is generated by the solution of the inverted forms of Eqs. (4) and (5), i.e.,

$$g^{11}\frac{\partial^2 x}{\partial \xi^2}+g^{22}\frac{\partial^2 x}{\partial \eta^2}+2g^{12}\frac{\partial^2 x}{\partial \xi \partial \eta}+f^1\frac{\partial x}{\partial \xi}+f^2\frac{\partial x}{\partial \eta}=0 \quad (6)$$

$$g^{11}\frac{\partial^2 y}{\partial \xi^2}+g^{22}\frac{\partial^2 y}{\partial \eta^2}+2g^{12}\frac{\partial^2 y}{\partial \xi \partial \eta}+f^1\frac{\partial y}{\partial \xi}+f^2\frac{\partial y}{\partial \eta}=0 \quad (7)$$

where

$$g^{11}=(x_\eta^2+y_\eta^2)/g, \quad g^{12}=-(x_\xi x_\eta+y_\xi y_\eta)/g$$
$$g^{22}=(x_\xi^2+y_\xi^2)/g, \quad g=(x_\xi y_\eta-x_\eta y_\xi)^2 \quad (8)$$

and the subscripts ξ and η denote derivatives. For the calculations presented herein, the grid-control functions have been assigned the following forms

$$\begin{aligned} f^1/2g^{11}&=A_1, && Z_1\geq 3/2\\ &=-A_1\sin\pi Z_1, && 0\leq Z_1\leq 3/2\\ &=A_2\sin\pi Z_2, && 0\leq Z_2\leq 3/2\\ &=-A_2, && Z_2\geq 3/2 \end{aligned} \quad (9)$$

with

$$Z_1=\frac{\xi_2-\xi}{\xi_2-\xi_1} \qquad Z_2=\frac{\xi-\xi_2}{\xi_3-\xi_2}$$

$$f^2/2g^{22}=-A_3$$

where ξ_1 and ξ_3 correspond to the leading and trailing edges, respectively. The positive constant values of A_1, A_2, and A_3 can be selected to yield the desired grid concentrations near the leading and trailing edges and close to the plate.

Using these rather simple control functions, Eqs. (6) and (7) can be locally linearized in each numerical element shown in Fig. 1, as

$$\frac{\partial^2 x}{\partial \xi^2}=2a\frac{\partial x}{\partial \xi} \quad (10)$$

$$\frac{\partial^2 y}{\partial \eta^2}=2b\frac{\partial y}{\partial \eta} \quad (11)$$

where a and b are constants defined by

$$a=-\frac{f^1}{2g^{11}}\bigg|_P \qquad b=-\frac{f^2}{2g^{22}}\bigg|_P \quad (12)$$

Equations (10) and (11) were solved analytically in each numerical element. A set of algebraic equations is then obtained by evaluating the analytic solutions at the central node P of the local element:

$$x_P=\frac{e^a x_U+e^{-a}x_D}{e^a+e^{-a}} \quad (13)$$

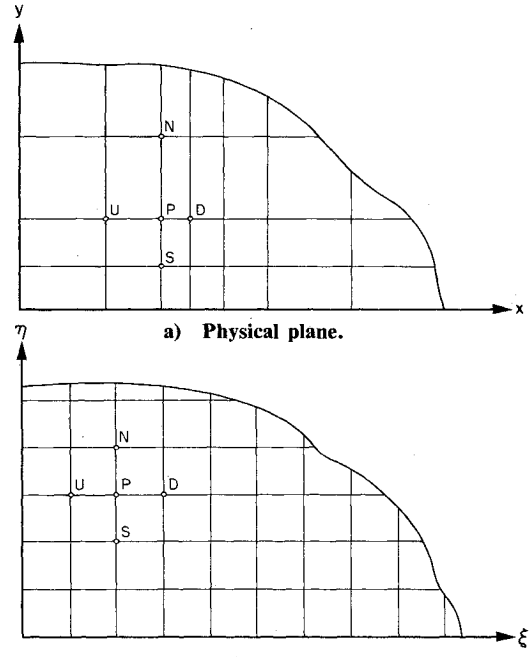

Fig. 1 Node arrangement in grid generation.

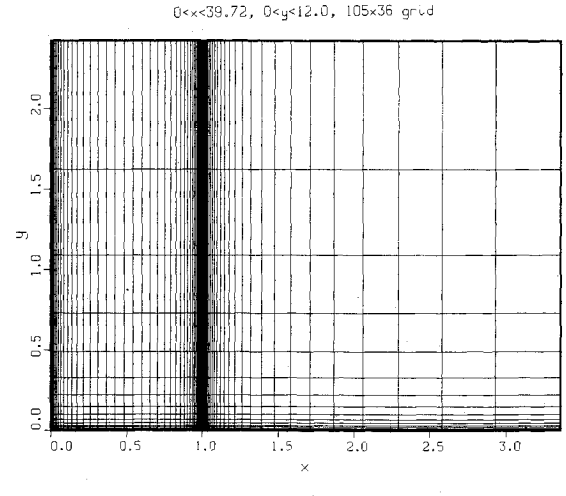

Fig. 2 A partial view of the numerical grid ($0<x<1.0$ is the plate).

$$y_P=\frac{e^b y_S+e^{-b}y_N}{e^b+e^{-b}} \tag{14}$$

The assembly of Eqs. (13) and (14) for all numerical elements results in a set of simultaneous algebraic equations which can be solved directly by a tridiagonal-matrix algorithm. Also, the first derivatives which appear in the geometric coefficients of the coordinate transformation can be written as

$$x_\xi\Big|_P=\frac{2a}{e^{2a}-e^{-2a}}\,(x_D-x_U) \tag{15}$$

$$y_\eta\Big|_P=\frac{2b}{e^{2b}-e^{-2b}}\,(y_N-y_S) \tag{16}$$

A partial view of a typical numerical grid, generated with $A_1=0.15$, $A_2=0.1$, and $A_3=0.2$, is shown in Fig. 2. Here, 105 x stations are used in the domain $0<x<39.72$, and with $\xi=1$ at the leading edge ($x=0$), $\xi=61$ at the trailing edge ($x=1$), and $\xi=105$ at $x=39.72$; and 35 y stations are used in the domain $0<y<12$, with $\eta=2$ on the plate ($y=0$), $\eta=36$ at the outer boundary ($y=12$), and the symmetry conditions $y(1)=-y(3)$ specified at $y=0$. In the following calculations, only a part of this grid is used, depending on the location of the boundaries of the solution domain. Also, to study grid dependence, alternate points in this grid were omitted in the x and y directions to obtain coarser grids.

C. Numerical Scheme

Using the coordinates described above, Eqs. (1) and (2) can be written in the transformed plane (ξ,η) as

$$g^{11}\frac{\partial^2 u}{\partial\xi^2}+g^{22}\frac{\partial^2 u}{\partial\eta^2}=\left(\frac{R}{J}\,b_1^1u-f^1\right)\frac{\partial u}{\partial\xi}+\left(\frac{R}{J}\,b_2^2v-f^2\right)\frac{\partial u}{\partial\eta}+R\frac{\partial u}{\partial t}+\frac{R}{J}\,b_1^1\frac{\partial p}{\partial\xi} \tag{17}$$

$$g^{11}\frac{\partial^2 v}{\partial\xi^2}+g^{22}\frac{\partial^2 v}{\partial\eta^2}=\left(\frac{R}{J}\,b_1^1u-f^1\right)\frac{\partial v}{\partial\xi}+\left(\frac{R}{J}\,b_2^2v-f^2\right)\frac{\partial v}{\partial\eta}+R\frac{\partial v}{\partial t}+\frac{R}{J}\,b_2^2\frac{\partial p}{\partial\eta} \tag{18}$$

and the equation of continuity [Eq. (3)] becomes

$$\frac{1}{J}\left[\frac{\partial}{\partial\xi}\,(b_1^1u)+\frac{\partial}{\partial\eta}\,(b_2^2v)\right]=0 \tag{19}$$

where

$$b_1^1=y_\eta,\quad b_2^2=x_\xi,\quad J=x_\xi y_\eta$$

$$g^{11}=1/x_\xi^2,\quad g^{22}=1/y_\eta^2$$

Equations (17) and (18) may be written in the standard form

$$g^{11}\phi_{\xi\xi}+g^{22}\phi_{\eta\eta}=2A_\phi\phi_\xi+2B_\phi\phi_\eta+R\phi_t+S_\phi \tag{20}$$

where

$$\phi\equiv u,v$$

$$A_u=A_v=\tfrac{1}{2}\{(R/J)b_1^1u-f^1\},\quad B_u=B_v=\tfrac{1}{2}\{(R/J)b_2^2v-f^2\}$$

$$S_u=(R/J)b_1^1p_\xi\qquad S_v=(R/J)b_2^2p_\eta$$

These are solved by the finite-analytic method of Refs. 8 and 9 assuming that the pressure field is known. The continuity equation [Eq. (19)] is then used to update the pressure field. These procedures are outlined in the following.

The Finite-Analytic Method

In the finite-analytic approach, Eq. (20) is first locally linearized in each numerical element ($\Delta\xi=\Delta\eta=1$) by evaluating the coefficients of the convective terms at the interior node P (Fig. 3), i.e.,

$$g_P^{11}\phi_{\xi\xi}+g_P^{22}\phi_{\eta\eta}=2(A_\phi)_P\phi_\xi+2(B_\phi)_P\phi_\eta+R\phi_t+(S_\phi)_P \tag{21}$$

Introduction of coordinate-stretching functions $\xi^*=\xi/\sqrt{g_P^{11}}$, $\eta^*=\eta/\sqrt{g_P^{22}}$ then leads to

$$\phi_{\xi^*\xi^*}+\phi_{\eta^*\eta^*}=2A\phi_{\xi^*}+2B\phi_{\eta^*}+R\phi_t+(S_\phi)_P \tag{22}$$

where $A=(A_\phi)_P/\sqrt{g_P^{11}}$, $B=(B_\phi)_P/\sqrt{g_P^{22}}$. For a local element with dimensions $\Delta\xi^*=h=1/\sqrt{g_P^{11}}$, $\Delta\eta^*=k=1/\sqrt{g_P^{22}}$, Eq. (22) may be written

$$\phi_{\eta^*\eta^*}=2B\phi_{\eta^*}+G \tag{23}$$

where $G=(2A\phi_{\xi^*}-\phi_{\xi^*\xi^*}+R\phi_t+S_\phi)_P$ is the source function evaluated at the node P. In the present study, the ξ^* derivatives are approximated by an exponential-linear scheme, while the time derivatives are approximated by a backward-difference formula, such that

$$2A\phi_{\xi^*}-\phi_{\xi^*\xi^*}=(C_U+C_D)\phi_P-C_U\phi_U-C_D\phi_D \tag{24}$$

with

$$C_U=\frac{Ae^{Ah}}{h\sinh Ah}\qquad C_D=\frac{Ae^{-Ah}}{h\sinh Ah}$$

$$(R\phi_t)_P=(R/\tau)(\phi_P-\phi_P^{n-1})$$

where the subscripts U and D denote the upstream and downstream nodal values, respectively, superscript $(n-1)$ denotes the nodal value at the previous time step, and τ is the time step.

When the boundary conditions along the sides of the element are expressed in terms of the nodal values, Eq. (23) can be solved analytically in each numerical element. A finite-analytic discretization formula is then obtained by evaluating the analytic solution at the point P in terms of surrounding nodal values:

$$\phi_P=C_N\phi_N+C_S\phi_S-C_PG \tag{25}$$

where

$$C_N=\frac{e^{-Bk}}{2\cosh Bk}\qquad C_S=\frac{e^{Bk}}{2\cosh Bk}\qquad C_P=\frac{k\tanh Bk}{2B}$$

By substituting the nonhomogeneous term G of Eq. (23) into Eq. (25), a six-point finite-analytic discretization formula for unsteady, two-dimensional, elliptic equations can be obtained:

$$\phi_P=\frac{1}{1+C_P[C_U+C_D+(R/\tau)]}\left[C_N\phi_N+C_S\phi_S+C_P\left(C_U\phi_U+C_D\phi_D+\frac{R}{\tau}\,\phi_P^{n-1}\right)-C_P(S_\phi)_P\right] \tag{26}$$

It is seen that ϕ_P depends upon ϕ_N and ϕ_S at the current station as well as the values at the upstream and downstream nodes ϕ_U and ϕ_D, and the values at the previous time step $(n-1)$. When the cell Reynolds number $2A$ becomes large, $C_U \to 2A/h$ and $C_D \to 0$, and Eq. (26) reduces to the partially parabolic formulation of Chen and Patel,[7] which used $C_U = 2A/h$ and $C_D = 0$. Thus, the extension of the partially parabolic method to a fully elliptic one is straightforward and if ϕ_D is obtained from the previous time step the same algorithms can be employed. Since Eq. (26) is implicit, both in time and space at the current station of calculation, its assembly for all elements leads to a set of simultaneous algebraic equations. These equations are solved directly by the tridiagonal-matrix algorithm.

Pressure Correction via Continuity Equation

If the pressure is known a priori, Eq. (26) can be employed directly to solve Eq. (20) for u and v. However, since the pressure is not known, it must be determined by requiring the velocity field to satisfy the equation of continuity. In the present study the SIMPLER algorithm of Patankar[10] is employed to update the pressure field.

The actual velocity field (u,v) is decomposed into a pseudovelocity field $(\hat{u},\hat{v})$ plus the pressure gradient terms contained in the source functions, i.e.,

$$u_d = \hat{u}_d - d_d(p_D - p_P)$$

$$v_n = \hat{v}_n - d_n(p_N - p_P) \tag{27}$$

where

$$d_d = \frac{(Rb_1^1)_d C_d}{J_d\{1 + C_d[C_U + C_D + (R/\tau)]_d\}}$$

$$d_n = \frac{(Rb_2^2)_n C_n}{J_n\{1 + C_n[C_U + C_D + (R/\tau)]_n\}}$$

and C_d and C_n are the finite-analytic coefficients C_P evaluated at the staggered velocity nodes d and n shown in Fig. 3. Note that the pseudovelocities contain no pressure terms, and can be evaluated directly from the information known at a previous iteration or time step. If we require the velocity field to satisfy the discretized equation of continuity, namely

$$(b_1^1 u)_d - (b_1^1 u)_u + (b_2^2 v)_n - (b_2^2 v_s) = 0 \tag{28}$$

an equation for pressure can be derived:

$$a_P p_P = a_d p_D + a_u p_U + a_n p_N + a_s p_S - \hat{D} \tag{29}$$

where

$$a_d = (b_1^1)_d d_d, \qquad a_u = (b_1^1)_u d_u$$

$$a_n = (b_2^2)_n d_n, \qquad a_s = (b_2^2)_s d_s$$

$$a_P = a_d + a_u + a_n + a_s$$

$$\hat{D} = (b_1^1 \hat{u})_d - (b_1^1 \hat{u})_u + (b_2^2 \hat{v})_n - (b_2^2 \hat{v})_s$$

The solution to Eq. (29) enables the pressure to be obtained directly from an estimated velocity field, and the slow convergence usually encountered in the SIMPLE alogorithm is avoided.

Although the guessed pressure field can be updated directly by Eq. (29), in practical applications the new pressure field may produce a velocity field which violates the equation of continuity. In order to improve this imperfect velocity field, the pressure-correction equation used in the SIMPLE algorithm is employed here, i.e.,

$$a_P p'_P = a_d p'_D + a_u p'_U + a_n p'_N + a_s p'_S - D^* \tag{30}$$

with

$$D^* = (b_1^1 u^*)_d - (b_1^1 u^*)_u + (b_2^2 v^*)_n - (b_2^2 v^*)_s$$

where (u^*,v^*) is the imperfect velocity obtained from the imperfect pressure field p^*, and $p' \equiv p - p^*$ is the pressure-correction. The improved velocity field based on this pressure-correction is then given

$$u_d = u_d^* - d_d(p'_D - p'_P)$$

$$v_n = v_n^* - d_n(p'_N - p'_P) \tag{31}$$

where the coefficients a_P, a_d, d_d, etc., are as defined in Eq. (29).

D. The Complete Solution Procedure

The overall numerical solution procedure for the present steady-flow calculations may be summarized as follows:

1) Construct the coordinate system and calculate the geometric coefficients b_j^i, g^{ij}, J, etc.

2) Specify the velocity profile at the initial station; set $p = 0$ everywhere initially.

3) Calculate the finite-analytic coefficients for pressure, pressure-correction, and momentum equations at the downstream station. Store only the finite-analytic coefficients for the pressure equation.

4) Solve the momentum equations based on the guessed pressure field to obtain the starred velocity field (u^*,v^*). The resulting system of algebraic equations is solved by tridiagonal-matrix algorithm.

5) Calculate the mass source D^*, and solve the pressure-correction equation by tridiagonal-matrix algorithm.

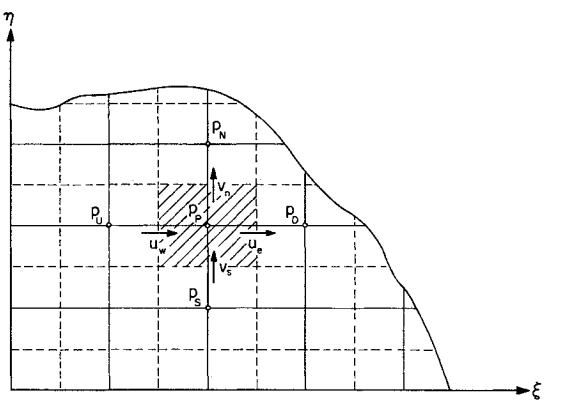

Fig. 3 Node arrangement and location of variables.

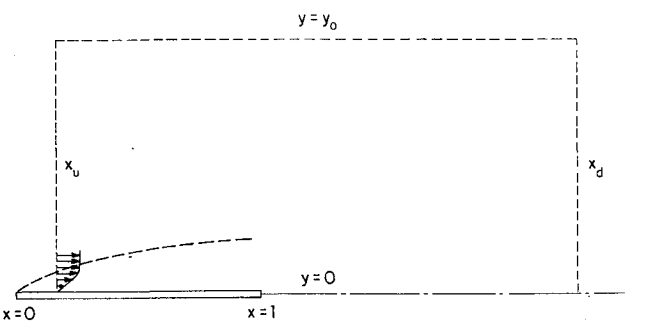

Fig. 4 Schematic of the solution domain.

6) Correct the velocity field using the velocity-correction formula, but do not correct the pressure field.

7) Calculate $\hat{D}$ based on the updated velocity field.

8) March to downstream station and repeat steps 3-7.

9) After reaching the most downstream station, solve the pressure equation by tridiagonal-matrix algorithm. Several sweeps *from downstream to upstream* are used to update the pressure field.

10) Return to step 2 and repeat steps 2-9 with the updated pressure field for several sweeps until both the pressure and velocity fields have converged.

III. Influence of Solution Domain

For the flow in the trailing-edge region, we seek a solution in the domain shown schematically in Fig. 4, i.e.,

$$x_u < x < x_d \qquad 0 \le y \le y_0$$

where the subscripts denote the upstream, downstream, and outer boundaries, respectively. The following boundary conditions are applied at the edges of the domain:

Upstream:	$x = x_u$;	$u(y)$ from Blasius, $v_x = 0$
Downstream:	$x = x_d$;	$p_x = u_{xx} = v_{xx} = 0$
Plate:	$y = 0$, $x < 1$;	$u = v = 0$
Wake centerline:	$y = 0$, $x > 1$;	$u_y = v = 0$
Outer:	$y = y_0$;	$u = 1$, $p = 0$

With the exception of the specification of the normal velocity v at the upstream station x_u, these boundary conditions require no comment. Systematic studies were first conducted with different distributions of the normal velocity at x_u. These revealed that the calculated pressure field was rather sensitive to the distribution of v *outside* the boundary layer. It has been suggested by Rubin and Reddy[11] that the assumption of zero streamwise gradient, $v_x = 0$, is perhaps the most appropriate since it is consistent with the boundary-layer approximations and ensures irrotationality of the flow outside the boundary layer. We have also adopted this procedure. The profiles of v calculated with this assumption were found to be in excellent agreement with the Blasius solution inside the boundary layer. However, from the results to be presented, it will be seen that this assumption is inconsistent with the full Navier-Stokes equations and leads to a local influence of the initial conditions on the solutions.

With regard to the size of the calculation domain, most previous numerical solutions of the trailing-edge problem (see, for example, Ref. 11 and 12) have used $x_u = 0.5$ and $x_d = 1.5$, with y_0 of the order of 0.2-0.4. Saint-Victor and Cousteix,[12] who used $y_0 = 0.224$ and 0.336, observed that the calculated pressure distribution on the plate and along the wake centerline was sensitive to the location of the outer boundary. In the present study, therefore, we have varied the locations of the boundaries x_u, x_d, and y_0 over a wide range to study the influence of the size of the solution domain. The solutions were examined with respect to all details, including the shapes of the velocity profiles in the boundary layer and the wake. In the interest of brevity, however, we shall present only three quantities which are of special interest, namely the pressure coefficient p on the plate and along the wake centerline, the skin-friction coefficient $\frac{1}{2}C_f\sqrt{R}$ at the plate, and the variation of velocity u_c along the wake centerline. Finally, we note that all calculations correspond to a $R = 10^5$, the value used by most previous investigators.

A. Convergence and Grid Dependence

Two important measures of the performance of the numerical method are the number of iterations required to obtain a converged solution and the influence of the grid. The most critical quantity to be examined in this regard is the pressure distribution since it is much more sensitive than either the friction coefficient or the velocity field.

Figure 5 shows the convergence of pressure in a typical calculation. It is seen that the solution converges in about 40

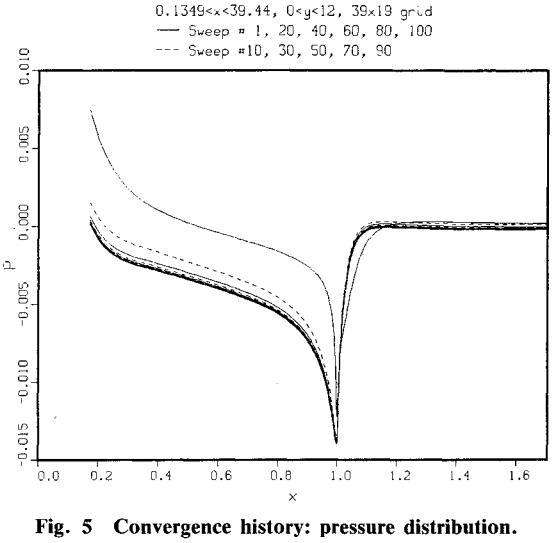

Fig. 5 Convergence history: pressure distribution.

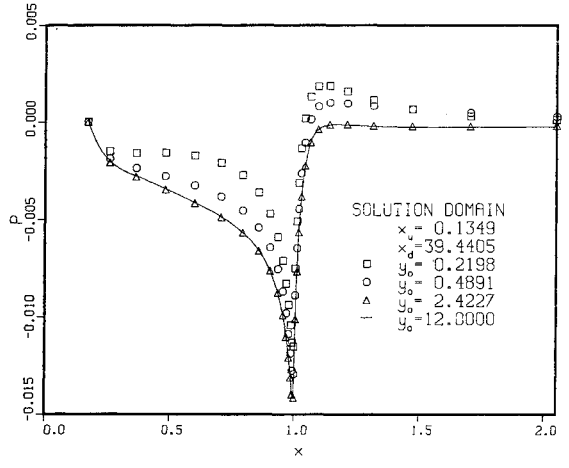

a) Pressure distribution.

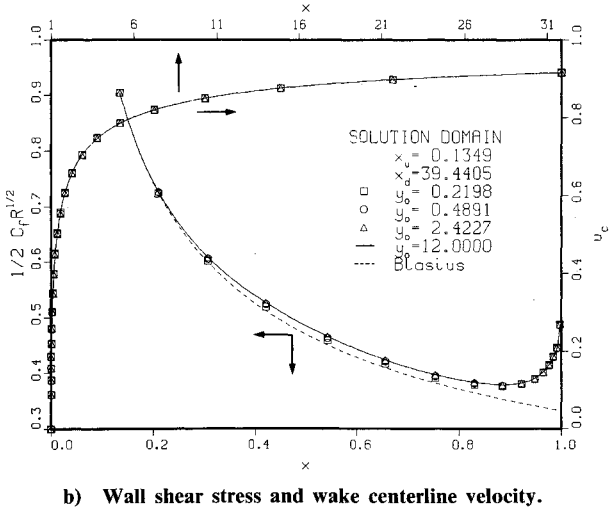

b) Wall shear stress and wake centerline velocity.

Fig. 6 Influence of outer boundary.

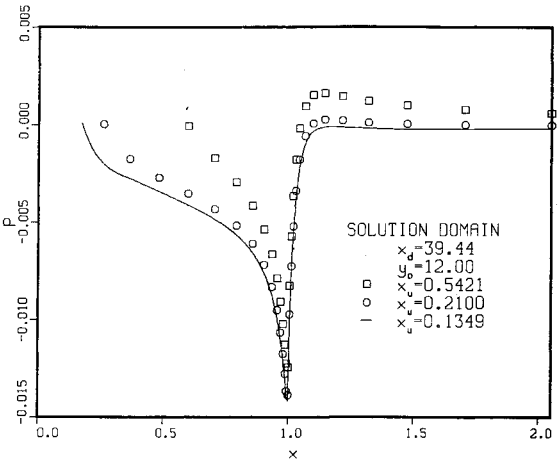

a) Pressure distribution.

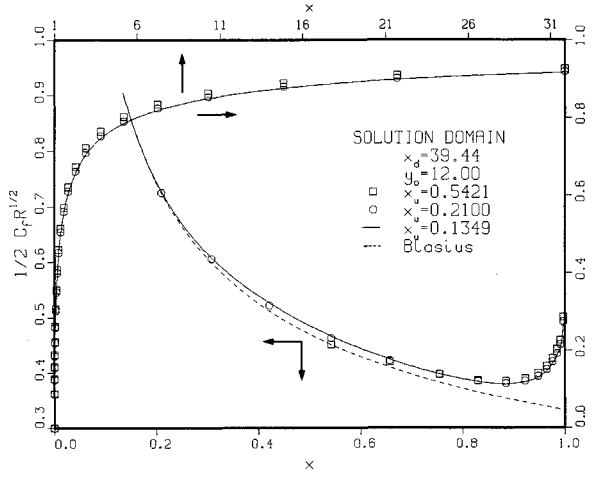

b) Wall shear stress and wake centerline velocity.

Fig. 7 Influence of upstream boundary.

iterations. This relatively rapid convergence is due to the downstream-to-upstream sweep in the solution of the pressure equation which transmits the pressure information upstream much more rapidly than in the downstream-marching techniques used previously.

Calculations were performed with three different (x,y) grids in the solution domain $0.12<x<40$, $0<y<12$, namely (77×36), (58×28), and (39×19). Refinement of the grid led to diminishing incremental changes in pressure, but the two finer grids gave identical friction coefficients and velocity distributions. In view of this, the final results presented in Sec. IV were obtained with the finest grid, which is shown in Fig. 2, but the calculations to study the influence of domain size discussed in the remainder of this section were performed with the coarse grid.

B. Influence of Outer Boundary, y_0

With upstream and downstream boundaries located at $x_u=0.1349$ and $x_d=39.44$, solutions were obtained with four different values of y_0, ranging from 0.2198, which corresponds to that used in Ref. 12, to as large as 12.0. From the results presented in Fig. 6, it is clear that the friction coefficient and the wake centerline velocity are not very sensitive to the location of the outer boundary, but the pressure distribution shows a systematic dependence. The trend with increasing y_0 is similar to that observed in Ref. 12, but the present results indicate that the outer boundary must be located at distances of the order of two plate-lengths in order to capture the viscous-inviscid interaction and for the solution to be independent of the location of this boundary.

C. Influence of Downstream Boundary, x_d

Calculations were performed with the downsteam boundary located at several positions, ranging from $x_d\sim1.5$, as in some previous calculations, to $x_d\sim40$, which is in the far wake. It was observed that the flow over the plate and in the near wake was quite insensitive to the choice of x_d in this range but the pressure distribution in the wake showed small but consistent differences. This suggested that $x_d\sim1.5$ may be too small to insure a proper prediction of the pressure recovery in the far wake.

D. Influence of Upstream Boundary, x_u

The influence of the location of the upstream boundary is shown in Fig. 7. We note a systematic and quite dramatic dependence of the solution on the choice of this boundary. The skin friction coefficient departs gradually from the Blasius solution and the increase in C_f above the Blasius value near the trailing edge is somewhat smaller as the initial conditions are applied further upstream. Also, the wake centerline velocity recovers more slowly with decreasing x_u. However, the most dramatic effect of changing x_u is seen in the pressure distribution.

At this point it is important to note a general feature of all the solutions presented thus far. Examination of the pressure distribution shown in Figs. 5–7 reveals that the predicted pressure at the most upstream station is always zero and, as the initial station is moved upstream, there is a sharp drop in pressure over a short distance. Both of these features are due to the assumed initial conditions. The zero pressure at the initial station is consistent with the boundary-layer type (u from Blasius, $v_x=0$) initial conditions imposed, and the drop in pressure simply indicates that these are not consistent with the subsequent solutions of the full Navier-Stokes equations. Thus, it appears that a complete solution, with no dependence on the initial conditions, can be obtained only if the flow over the leading edge is also resolved. Although the present calculation method can be extended to include the leading edge, for the purpose of this paper all subsequent calculations were performed with $x_u=0.1224\sim0.1349$, depending upon the grid used, since Fig. 7a indicates an approach to a unique solution as the initial station is moved upstream and Fig. 7b shows little influence, if any, of the initial conditions on the velocity field and friction on the plate for $x_u<0.2$.

IV. Large-Domain Solutions and Comparisons with Other Methods

From the results presented in the previous section it is clear that the solution of the Navier-Stokes equations for the trailing-edge flow depends upon the size of the computation domain, and that the domains used by previous investigators have not been large enough to obtain domain-independent solutions. Although the present method recovered the main features of the previous solutions when comparable solution domains were used, detailed comparisons are not particularly useful. Instead, it is of interest to compare our results with the largest solution domain, which are independent of the domain size, with those obtained by other, quite different methods, namely, the triple-deck formulation and interactive boundary-layer theory. For this purpose, we have selected the triple-deck results of Melnik and Chow[4] and Veldman and van de Vooren,[5] which are essentially identical but improvements upon the previous ones of Jobe and Burggraf,[3] and the interactive solutions of Veldman.[13] Initially, it was thought that our results with the largest solution domain should agree with the results of these two approaches. However, this turned out not to be the case for reasons we shall now explore.

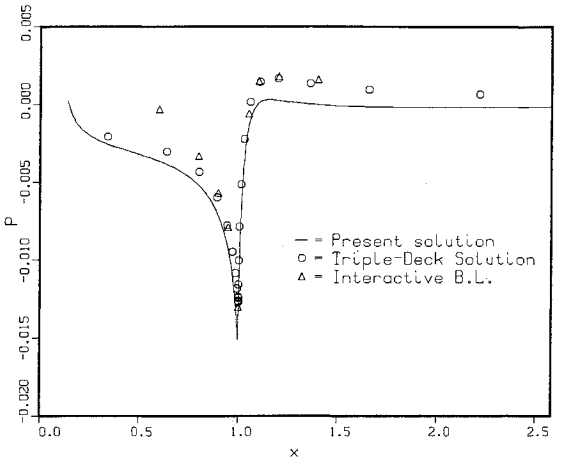

a) Pressure distribution.

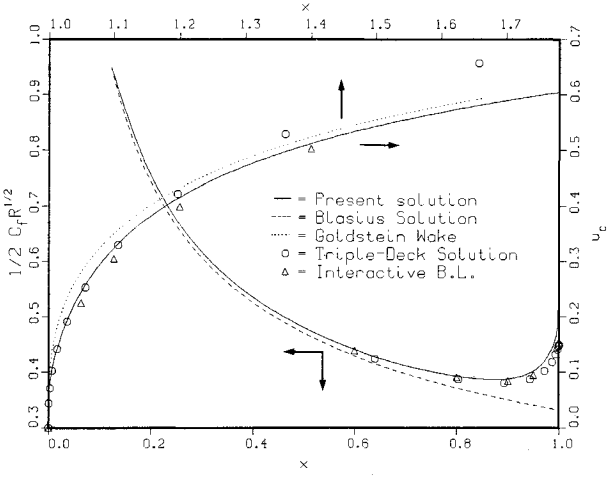

b) Wall shear stress and wake centerline velocity.

Fig. 8 Comparisons with other solutions.

First, we recognize that the triple-deck and the interactive boundary-layer calculations are also numerical solutions and, as such, involve a choice of solution domains and boundary conditions, in addition to the numerical schemes. Veldman[13] has presented solutions for $R=10^5$. He assumed that the interaction is confined to the region $0.5<x<1.5$, and imposed the Blasius solution upstream and zero pressure-gradient condition, or its equivalent, downstream. The boundary-layer equations were then solved in the inverse mode in the region $0<y<7\delta^*/L$, where δ^* is the displacement thickness. At the trailing edge, this corresponds to $0<y<0.038$. Three (x,y) grids were employed: 41×21, 81×41, and 121×61, and the solution was found to change with grid refinement. For example, the corresponding trailing-edge pressure was -0.0116, -0.0126, and -0.0130. Melnik and Chow, on the other hand, solved the boundary-layer equations, appropriate for the lower deck, in the region $-17<x^*<20.8$, $0<y^*<8$, where x^* and y^* are the transformed triple-deck coordinates. For $R=10^5$, this corresponds approximately to $0.10<x<2.10$, $0<y<0.014$. The Blasius solution again provided the initial conditions. At the downstream boundary, the solution was matched to the $u_c\sim x^{1/3}$ intermediate-wake solution of Goldstein.[14] Subsequently, we shall see that this is responsible for some of the differences between the present results and the commonly accepted triple-deck results. In both the triple-deck and the interactive boundary-layer calculations, the boundary conditions at the outer edge of the solution domain are established

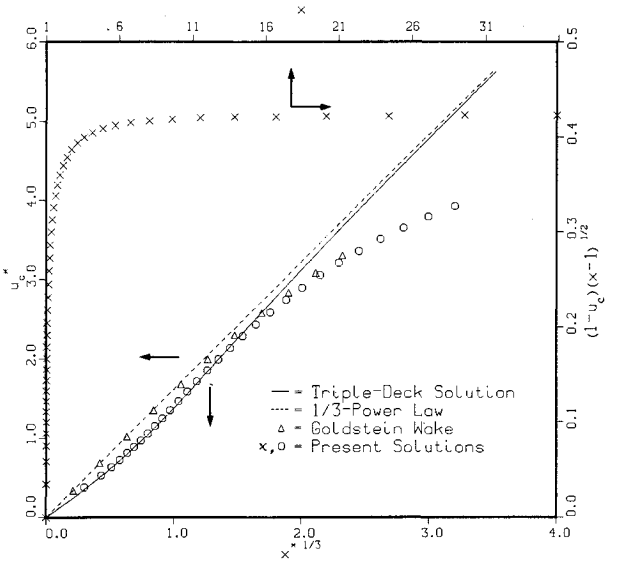

Fig. 9 Wake centerline velocity in triple-deck and defect coordinates.

through compatibility with an inviscid solution that includes the boundary-layer and wake displacement effects. These details of the previous solutions have to be taken into consideration in evaluating the comparisons with the present results presented herein.

The three sets of results are compared in Fig. 8. It is evident that the present method predicts a lower trailing-edge pressure (-0.0152) than the triple-deck value of -0.0128 and the value of -0.0130 obtained by Veldman[13] with the finest grid. Further differences are observed in the pressure distribution over the plate and in the wake. The three solutions are in somewhat better agreement with respect to the shear stress on the plate, but the wake centerline velocity shows systematic differences.

On the plate, the difference between the present results and those of Veldman[13] are primarily due to the different initial conditions. In Veldman's interactive calculations, the pressure is assumed to be zero at $x=0.5$, whereas the present calculations indicate that the interaction penetrates further upstream. Indeed, as shown in Fig. 7a, the present method predicted results very similar to those of Veldman when the initial conditions were applied at $x=0.5$. The earlier departure of the friction coefficient from the Blasius value in the present solutions confirms the greater extent of the interaction.

In the wake, Fig. 8a shows that the present calculations predict a faster recovery to ambient zero pressure with a much smaller positive over-shoot pressure, while the triple-deck and interactive boundary-layer solutions predict a slower recovery and greater overshoots. These differences are consistent with those in the wake centerline velocity distributions shown in Fig. 8b and replotted in Fig. 9 in triple-deck coordinates, $x^*=\lambda^{5/4}R^{3/8}x$ and $u_c^*=\lambda^{-1/4}R^{1/8}u_c$, with $\lambda=0.332$, the constant in the Blasius solution. Also included is the classical, noninteractive, parabolic solution of Goldstein.[14]

Figure 9 clearly shows that the present calculations are in agreement with the Goldstein solution[14] beyond a certain distance form the trailing edge. In the near wake, we observe departures from the Goldstein solution identical with those predicted by the triple-deck calculations. However, it is also clear that the Goldstein solution departs from the intermediate $x^{1/3}$ power behavior, assumed for the downstream matching condition in the triple-deck calculations, well before the station ($x^*=20.8$, $x=2.10$) where Melnik and Chow[4] matched their solutions with the $x^{1/3}$ wake. Since the pressure distribution in the triple-deck calculations is criti-

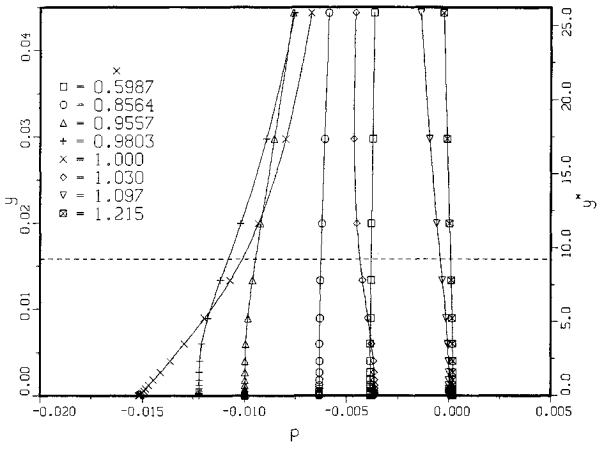

Fig. 10 Pressure distribution normal to the plate: - - - -, Blasius thickness at the trailing edge.

cally dependent on the downstream boundary conditions, it appears that the differences between the present results and those of the triple-deck calculations (in both the pressure and wake centerline velocity distributions), originate from the improper numerical treatment of the downstream flow in the latter method. In other words, requiring the velocity to vary as $x^{1/3}$ far downstream implies pressure gradients that are not present if the correct asymptotic conditions in the far wake are imposed. These pressure gradients when integrated, lead to the larger pressures in the near wake, and since the trailing-edge pressure is used to match the pressure distribution on the plate, the error propagates upstream.

The behavior of the wake centerline velocity at large distances from the trailing edge is illustrated in Fig. 9. It is seen that the present large-domain solution correctly predicts the well known asymptotic velocity-defect result $(1-u_c) \sim (1-x)^{-1/2}$. It is also interesting to note that, at the Reynolds number considered here, the asymptotic state is achieved only after a distance of the order of 15 plate lengths from the trailing edge.

The preceding observations do not of course explain the differences between the present results and those of the interactive boundary-layer method of Veldman.[13] However, as noted earlier, Veldman assumed that the viscous-inviscid interaction is confined to the region $0.5<x<1.5$. We have already commented on the influence of the upstream boundary. In addition to this effect, Fig. 9 suggests that the downstream boundary also may not be far enough to capture the interaction. Furthermore, it should be recognized that Veldman's solutions are those of the boundary-layer equations while the present solutions are those of the complete Navier-Stokes equations and take into account the variation of pressure through the viscous domain.

In order to explore the assumptions underlying the triple-deck and interactive boundary-layer formulations, it is instructive to examine the variation of pressure in the normal direction predicted by the present calculations. This is shown in Fig. 10. It shoud be pointed out that this figure shows only a small part ($y<0.04$) of the total solution domain, which extends to $y=12$, where $p=0$ is enforced. Also shown for reference, is the thickness of the Blasius boundary layer at the trailing edge and the triple-deck variable $y^*=\lambda^{3/4}R^{5/8}y$. Clearly, the present results confirm the assumption of constant pressure in the lower deck of the triple-deck formulation. Although the bulk of the pressure variation occurs in the inviscid flow outside the boundary layer, there is a region of the order of one boundary-layer thickness on either side of the trailing edge, in which significant variations of pressure are observed within the boundary layer. This is the region in which the assumptions of interactive boundary-layer theory are not valid.

Finally, we note that the present calculations were performed with a numerical scheme appropriate for the full Navier-Stokes equations. However, for the simple case of a flat plate and the large Reynolds number of 10^5 considered here, there is practically no difference between the Navier-Stokes solutions and those of the partially parabolic equations because the effect of longitudinal diffusion neglected in the latter is confined to a region very close to the trailing edge which is too small to be resolved even by the finest grid. This was verified by numerous calculations with the reduced equations, which, as explained in Sec. II, could be accomplished quite simply by using the limiting forms of the coefficients in Eq. (24). The two solutions will deviate however, as the Reynolds number decreases. Furthermore, the present numerical scheme can be used for other, more complex shapes, with or without separation and for the leading edge problem.

V. Conclusions

The present study may be summarized as follows:

1) It has been shown that numerical solutions of the flow over the trailing edge are quite sensitive to the size of the solution domain. Most previous studies have used domains which were too small in all directions to obtain a domain-independent solution.

2) The present large-domain solution is in agreement with the triple-deck solutions in the boundary layer ahead of the trailing edge and in the near wake, with Goldstein's intermediate wake solution,[14] and with the asymptotic wake solution.

3) At a Reynolds number of 10^5, the wake reaches an asymptotic state after a distance of about 15 plate lengths from the trailing edge.

4) The present solution confirms the assumptions concerning the constancy of pressure in the lower deck in the triple-deck formulation, and the validity of the interactive boundary-layer formulation outside a region of the order of one boundary-layer thickness around the trailing edge.

5) The dependency of the numerical solutions of the assumed initial conditions for the normal velocity can best be removed by considering the flow over the entire plate, i.e., by also including the leading edge within the computational domain and prescribing uniform-flow conditions far upstream. Such an extension of the present solutions is in progress.

Acknowledgments

This research was supported by the Office of Naval Research under the Special (Accelerated Initiative) Focus Research Program in Ship Hydrodynamics, Contract N00014-83-K-0136.

References

[1]Stewartson, K., "On the Flow Near the Trailing Edge of a Flat Plate II," *Mathematicka*, Vol. 16, 1969, pp. 106–121.

[2]Messiter, A., "Boundary-Layer Flow Near the Trailing Edge of a Flat Plate," *SIAM Journal of Applied Mathematics*, Vol. 18, 1970, pp. 241–257.

[3]Jobe, C. E. and Burggraf, O. R., "The Numerical Solution of the Asymptotic Equations of Trailing-Edge Flow," *Proceedings of the Royal Society*, London, Vol. A340, 1974, pp. 91–111.

[4]Melnik, R. E. and Chow, R., "Asymptotic Theory of Two-Dimensional Trailing-Edge Flows," *Aerodynamic Analysis Requiring Advanced Computers*, NASA SP 347, 1975, pp. 177–249.

[5]Veldman, A. E. P. and van de Vooren, A. I., "Drag of a Finite Flat Plate," *Proceedings of the 4th International Conference on Numerical Fluid Dynamics*, Boulder CO; also, *Lecture Notes in Physics*, Springer-Verlag, NY, Vol. 35, 1974, pp. 423–430.

[6]McDonald, H. and Briley, W. R., "A Survey of Recent Work on Interacted Boundary Layer Theory for Flow with Separation," *Pro-*

ceedings of the 2nd Symposium on Numerical and Physical Aspects of Aerodynamic Flows, Long Beach, CA, Session 5, Paper 1, 1983.

[7]Chen, H. C. and Patel, V. C., "Calculation of Trailing-Edge, Stern and Wake Flows by a Time-Marching Solution of the Partially-Parabolic Equations," Iowa Institute of Hydraulic Research, Univ. of Iowa, IIHR Rept. 285, 1985.

[8]Chen, C. J. and Chen, H. C., "Development of Finite-Analytic Method for Unsteady Three-Dimensional Navier-Stokes Equations," Iowa Institute of Hydraulic Research, Univ. of Iowa, IIHR Rept. N232-IV, 1982.

[9]Chen, C. J. and Chen, H. C., "Finite-Analytic Numerical Method for Unsteady Two-Dimensional Navier-Stokes Equations," *Journal of Computational Physics*, Vol. 53, 1984, pp. 210–226.

[10]Patankar, S. V., *Numerical Heat Transfer and Fluid Flow*, McGraw Hill, 1980, pp. 113–137.

[11]Rubin, S. G. and Reddy, D. R., "Global Solution Procedures for Incompressible Laminar Flow with Strong Pressure Interaction and Separation," *Proceedings of the 2nd Symposium on Numerical and Physical Aspects of Aerodynamic Flow*, Long Beach, CA, Session 1, Paper 4, 1983.

[12]Saint-Victor, X. and Cousteix, J., "Calcul de l'Ecoulement au Voisinage du Bord de Fuite d'une Plaque Plane," CERT, ONERA, Toulouse, France, Rept. 57/2259, 1983.

[13]Veldman, A. E. P., "A Numerical Method for the Calculation of Laminar, Incompressible Boundary Layers with Strong Viscous-Inviscid Interaction," National Aerospace Lab., Amsterdam, the Netherlands, Rept. NLR TR 79023U, 1979.

[14]Goldstein, S., "Concerning Some Solutions of the Boundary Layer Equations in Hydrodynamics," *Proceedings of the Cambridge Philosophical Society*, Cambridge, England, Vol. 26, 1930, pp. 1–30.